Frontiers of Information Technology & Electronic Engineering
www.jzus.zju.edu.cn; engineering.cae.cn; www.springerlink.com
ISSN 2095-9184 (print); ISSN 2095-9230 (online)
E-mail: jzus@zju.edu.cn

A geographic information encryption system based on chaos-LSTM and chaos sequence proliferation*

Jia DUAN[1,2], Luanyun HU[1,2], Qiumei XIAO[†‡3], Meiting LIU[3], Wenxin YU[3]

[1]*Third Surveying and Mapping Institute of Hunan Province, Hunan Pro., Changsha 410000, China*

[2]*Hunan Engineering Research Center of Geographic information security and application, Hunan Pro., Changsha 410000, China*

[3]*School of Information and Electrical Engineering, Hunan University of Science and Technology, Hunan Pro., Xiangtan 411201, China*

[†]E-mail: 1959582421@qq.com

Received Nov. 7, 2023; Revision accepted Apr. 8, 2024; Crosschecked

Abstract: In response to the strong correlation between the chaotic system state and initial state and parameters in traditional chaotic encryption algorithms, which may lead to the periodicity of chaotic sequences, the Chaos-LSTM model is constructed by combining chaotic systems and LSTM neural networks. The chaos sequence proliferation (CSP) algorithm is constructed to address the problem that the limited computational accuracy of computers can lead to the periodicity of long chaotic sequences, making it unsuitable for encrypting objects with large amounts of data. Combining the above two, the geographic information encryption system based on Chaos-LSTM and CSP is proposed. Firstly, the Chaos-LSTM model is used to output chaotic sequences with high Spectral Entropy (SE) complexity. Then, a shorter chaotic sequence is selected and proliferated using the CSP algorithm to generate chaotic proliferation sequences that match the encrypted object, and a randomness analysis is conducted and testing is performed on it. Finally, using geographic images as encryption objects, the chaos proliferation sequence, scrambling, and diffusion algorithm are combined to form the encryption system, which is implemented in the ZYNQ platform. The system's excellent confidentiality performance and scalability are proved by software testing and hardware experiments, which can be used for the confidentiality peers of various encryption objects with outstanding application value.

unedited

Key words: Chaos; LSTM; CSP; ZYNQ platform; Image encryption
https://doi.org/10.1631/FITEE.2300755 **CLC number:**

1 Introduction

With the deepening application of geographic information, various types of data are widely shared. The confidential information involved in geographic information data is extensive, and if leaked, it will lead to serious losses and harm. Therefore, it is crucial to provide a secure and inclusive communication system for different geographic information data. Encryption algorithms are the core of secure communication systems, and researchers have also proposed various encryption algorithms, such as the triple data encryption standard (Tezcan, 2022), elliptic curve cryptography (Ullah et al., 2023), the international data encryption algorithm (Sahu et al., 2016), fully homomorphic encryption (Martins et al., 2017), quantum key distribution (Cao et al., 2022), and so on.

In addition, chaotic systems, neural networks, and their combinations are all used for secure communication. Alexan et al. (2023) proposed a secure communication algorithm combining multiple maps. Gabr et al. (2023) proposed an image encryption algorithm that combines chaotic systems with unique image transformation techniques, promoting the application of chaotic encryption algorithms. Muril-

‡ Corresponding author
* Project supported by the Open Topic of Hunan Engineering Research Center of Geographic information security and application (No. HNGISA2023005)
ORCID: Qiumei XIAO, https://orcid.org/0009-0004-8924-5799
© Zhejiang University Press 2024

lo-Escobar et al. (2022) provided a data confidentiality scheme based on chaotic cryptography and sequence spread spectrum technology. Lin et al. (2022) proposed using a memristor ring neural network to encrypt medical images. Based on the Takagi–Sugeno fuzzy neural network, Yan et al. (2023) designed a synchronization controller for image encryption. Xu et al. (2022) proposed a method for constructing multiple hash index chains based on a fractional order chaotic Hopfield neural network (HNN). Based on convolutional neural networks and chaos, Man et al. (2021) studied a dynamic adaptive diffusion encryption algorithm. Gonzalez-Zapata et al. (2023) and De la Fraga et al. (2023) studied the implementation method and topology of the Echo State Neural Network (ESNN), using an improved ESNN to predict chaotic time series and enhancing the hardware of ESNN using the Field Programmable Gate Array (FPGA). Neural networks with learning capabilities can generate new sequences with chaotic characteristics by learning from existing chaotic time series. The different initial states of chaos systems correspond to different periods, and their period lengths may be very short, which, to some extent, reduces the confidentiality of chaos encryption systems. In response to this issue, this paper combines chaotic systems and LSTM neural networks to construct the Chaos-LSTM model. By using LSTM neural networks to learn the characteristics of chaotic systems and generating new chaotic sequences through trained LSTM neural networks, the potential periodic risks of chaotic systems are avoided.

Chaos systems and neural networks with excellent secure communication performance have been proven by many researchers. However, further research is needed to develop secure algorithms that generate adaptive data volumes when faced with multiple secure objects. Due to the computational accuracy and performance of existing computers being unable to perform completely ideal simulation solutions, most chaos systems implemented with limited accuracy may have properties that deviate from their theoretical results (Teh et al., 2020; Wan et al., 2020). Moreover, the limited computational accuracy of computers can ultimately lead to periods in chaos sequences. The longer the output chaotic sequence of a chaotic system, the greater the possibility of periodicity. How to make chaos sequences have longer periods and better randomness is the key to designing chaotic encryption algorithms (Chen et al., 2020; Irfan et al., 2020). To address this issue, this paper proposes chaos sequence proliferation (CSP), which proliferates the chaos sequences through local mean sequences and cyclic XOR operations. With only a small number of chaotic sequences, sufficient chaotic sequences for encryption can be generated without the need for chaotic systems to generate growth sequences, avoiding the potential periodicity caused by excessively long chaotic sequences.

To demonstrate the actual application effect, Liu et al. (2024) discretized the memristor on DSP and implemented a hyperchaotic mapping encryption algorithm. A novel pseudo-random number generator for encryption was developed by Yu et al. (2022) using FPGA to achieve memristor HNN. Tlelo-Cuautle et al. (2020) implemented hopfield and hindmarsh-rose neurons for chaotic image encryption on FPGA. The application of FPGA has promoted the implementation of secure communication algorithms for offline applications in various applications. This paper also implements the designed encryption system on the ZYNQ hardware platform.

In summary, this paper proposes a geographic information encryption system based on Chaos-LSTM and CSP. The Chaos-LSTM model and CSP algorithm constructed in this paper can further enhance the randomness of the chaos sequence on the basis of the chaos system. Only a part of the output sequence of the chaos system should be selected, avoiding the encryption performance deficiency caused by the low complexity of the chaos sequence.

The remaining sections of this paper are organized as follows: in Section 2, a Chaos-LSTM model is constructed and the complexity of its output sequence is analyzed. In Section 3, the CSP algorithm is designed. The SE complexity (Xiong et al., 2021) calculation, TestU01 tests (De la Fraga et al., 2021), and the National Institute of Standards and Technology (NIST) tests (Pareschi et al., 2012) are performed on the proliferation sequences. In Section 4, taking geographic information images as the object, an image encryption system is constructed using a secret key, the Chaos-LSTM model, the CSP algorithm, the scrambling and diffusion algorithm, and the encryption performance of the system is analyzed. In Section 5, the designed encryption system is implemented in

unedited

ZYNQ. Section 6 provides the main conclusions and future research directions of this work.

2 Construction of Chaos-LSTM Model

2.1 Chaos system

Lorenz established the Lorenz system while studying atmospheric convection models and first published research on chaos theory (Lorenz, 1963). Since then, the Lorenz system has been continuously discussed and cited, becoming a classic chaos system used to describe chaos phenomena. The chaos system used in this paper is a simplified Lorenz system, the mathematical model of which is shown in Eq. (1).

$$\begin{cases} \dot{x} = 10(y - x) \\ \dot{y} = (24 - 4c)x - xz + cy \\ \dot{z} = xy - 8z / 3 \end{cases}, \quad (1)$$

where, x, y, z are the system state variables and c is the system parameter. When $c \in [-1, 7.75]$, the simplified Lorenz system is in a chaotic state and the x, y, z dimensions of the system output chaos sequences $x(t), y(t), z(t)$. It should be noted that, although the chaos system used in this paper is the Lorenz system, this does not mean that the chaos system can only use the Lorenz system; other chaos systems with 2-D or above chaos sequence outputs can also be used.

2.2 LSTM

The LSTM neural network is a special recurrent neural network with time-recursive characteristics that can effectively handle long-term dependency problems, and the basic nodes are LSTM units. The standard LSTM unit consists of four structures, and its basic architecture is shown in Fig. 1 (Yu et al., 2019).

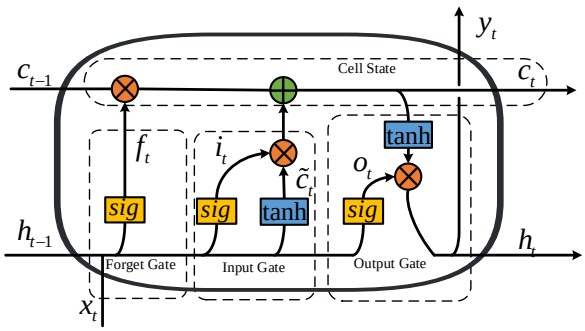

Fig. 1 Basic architecture of standard LSTM units.

In Fig. 1, x_t represents input, h_t represents cyclic information, y_t represents output, c_t represents cell state, $sig(\bullet)$ is the Sigmoid function, and $\tanh(\bullet)$ is the hyperbolic tangent function.

The forget gate, shown in Eq. (2), is used to control whether to discard information from the previous cell state.

$$f_t = sig(W_{fh} h_{t-1} + W_{fx} x_t + b_f). \quad (2)$$

The input gate, as shown in Eq. (3), determines the importance of input information.

$$\begin{aligned} i_t &= sig(W_{ih} h_{t-1} + W_{ix} x_t + b_i), \\ \tilde{c}_t &= \tanh(W_{\tilde{c}h} h_{t-1} + W_{\tilde{c}x} x_t + b_{\tilde{c}}). \end{aligned} \quad (3)$$

The cell state, as shown in Eq. (4), is used to store and transmit information, passing along the network throughout the entire time series.

$$c_t = c_{t-1} \square f_t + i_t \square \tilde{c}_t. \quad (4)$$

The output gate, as shown in Eq. (5), controls which information in the cell state will be transmitted to the output of the LSTM unit.

$$\begin{aligned} o_t &= \sigma(W_{oh} h_{t-1} + W_{ox} x_t + b_o), \\ h_t &= o_t \square \tanh(c_t), \\ y_t &= h_t. \end{aligned} \quad (5)$$

In Eqs. (2), (3), (4), and (5), W is weight, and b represents bias.

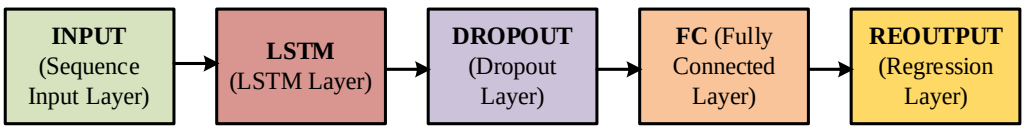

Fig. 2 LSTM recurrent neural network.

Based on the above LSTM units, an LSTM recurrent neural network is constructed in this paper. The input layer is the sequence input layer. The LSTM layer sets the number of LSTM units in the LSTM layer to 128, the state activation function to $\tanh(\bullet)$, and the gate activation function to $sig(\bullet)$. The dropout layer randomly discards input elements with 50% probability and sets the elements to zero. The fully connected layer uses the Xavier initializer (Jia et al., 2014) to initialize the weights and initialize

unedited

the bias with zero. The fifth layer is the regression output layer, which outputs regression sequence data. The input and output dimensions of each layer are set to 1, forming the LSTM recurrent neural network, as shown in Fig. 2.

2.3 Chaos-LSTM Model

Training the LSTM recurrent neural network through chaos sequences outputted from the Lorenz system, the neural network is transformed into a Chaos-LSTM model that can generate new chaos sequences. The chaotic sequence is input into it to predict the response of the data in the sequence, a new chaotic sequence of corresponding length is the output, and the network state of the model is updated. The Lorenz chaotic system and the LSTM neural network together constitute the Chaos-LSTM model. The flowchart of the Chaos-LSTM model processing is shown in Fig. 3.

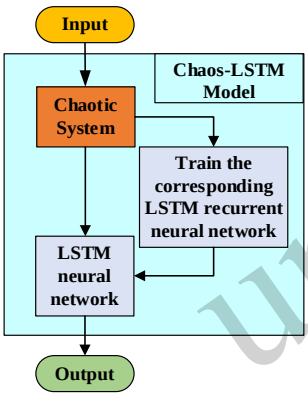

Fig. 3 The flowchart of Chaos-LSTM model processing.

In Fig. 3, the input is the initial values of state variables and the parameters of the Lorenz system, and the output is a new chaos sequence $x'(t)$. When the parameter is $c=2$ and the initial values are $x(0)=1, y(0)=2, z(0)=3$, the comparison between the chaos sequence $x(t)$ generated by the Lorenz system and the outputted new chaos sequence $x'(t)$ are shown in Fig.4 (a). As seen in Fig.4 (a), the new chaos sequence $x'(t)$ trained by the Chaos-LSTM model is different from the chaos sequence $x(t)$.

Complexity is a quantitative indicator of the randomness of chaotic sequences. Currently, the complexity classification algorithms for chaotic systems can be divided into two types: behavioral complexity and structural complexity. The SE complexity algorithm belongs to the structural complexity algorithm, which uses Fourier transform to obtain the corresponding spectral entropy value by combining the energy distribution in the Fourier transform domain with Shannon entropy (Xiong et al., 2021). SE complexity can represent the complexity of a signal sequence. The simpler the spectrum structure of the sequence, the closer the obtained SE measure value is to 0; that is, the smaller the complexity of the sequence is. The more complex the spectral structure of the sequence, the closer the SE measure value is to 1, indicating a higher complexity of the sequence.

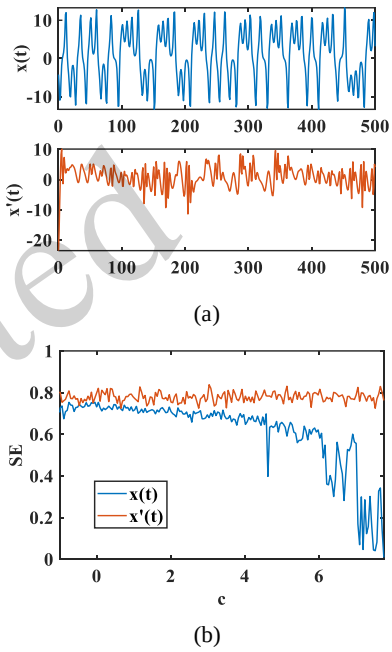

Fig. 4 (a) Comparison between chaos sequence $x(t)$ and new chaos sequence $x'(t)$; (b) SE complexity comparison with system parameter c changing

The SE complexity of the Lorenz system output sequence will change as system parameter c changes. Sequence $x(t)$ with a length of 500 and the corresponding sequence $x'(t)$ are selected for SE complexity comparison in Fig.4 (b). The SE complexity of the new chaos sequence $x'(t)$ is greater than that of the chaos sequence $x(t)$ under different system parameters c. Compared to the chaos sequence $x(t)$, the new chaos sequence $x'(t)$ is closer to a random sequence.

3 Chaos sequence proliferation

3.1 Chaos sequence proliferation algorithm

unedited

For chaos sequences generated by chaos systems, it is difficult to ensure that each sequence has a sufficiently large period and high complexity. Although the Chaos-LSTM model improves the randomness of the output sequence on the basis of the chaos system, the periodicity of the chaos sequence may still appear when the output sequence is long enough. To ensure that the chaos encryption sequence can match the data capacity of the encrypted object and have a longer periodicity, and maintain the randomness of the encryption sequence, this paper proposes the CSP algorithm. The algorithm only selects a portion of the chaos sequence and generates sufficient encrypted sequences through proliferation, to some extent avoiding the potential lack of encryption performance caused by the short periodicity of the chaos sequence.

The encryption of color images with size $3\times M\times N$ is taken as an example, which requires an encrypted sequence of length $3\times M\times N$. The implementation steps of the CSP algorithm are as follows:

Step 1: Input the parameter and the initial values of the chaos system, and iteratively solve the Lorenz system. Set the number of iterations to N, and generate three-dimensional floating-point chaos sequences $x(t), y(t), z(t)$ with length N.

Step 2: Input floating-point chaos sequence $x(t)$ into the trained LSTM neural network and output a new floating-point chaos sequence $x'(t)$ with the same length as chaos sequence $x(t)$.

Step 3: Convert floating-point chaos sequences $x'(t), y(t)$ with length N into integer chaos sequences $X(t), Y(t)$ through Eq. (6).

$$\begin{aligned} X(t) &= floor(x'(t)\times 2^n) \\ Y(t) &= floor(y(t)\times 2^n) \end{aligned} . \tag{6}$$

Among them, $floor(\bullet)$ is the rounding function, $n=16$. Eq. (6) represents moving the floating-point chaos sequence to the left by n bits before performing the rounding operation.

Step 4: Find all local extremum points in integer chaos sequence $X(t)$, and calculate the average values u_i of all adjacent local extremum points through Eq. (7).

$$u_i = \frac{v_i + v_{i+1}}{2}, 0 < i < N . \tag{7}$$

Step 5: Perform linear smooth interpolation on all local mean values to obtain an approximate local mean function sequence $u(t)$ with length N, and then convert floating-point sequence $u(t)$ to integer sequence $U(t) = floor(u(t))$.

Step 6: Introduce chaos sequence $Y(t)$, perform the XOR operation on local mean function sequence $U(t)$, sequence $Y(t)$, and sequence $X(t)$ to obtain CSP component DX_j.

$$DX_j(t) = U(t) \oplus Y(t) \oplus X(t) . \tag{8}$$

Step 7: Use the CSP component DX_j as the new chaos sequence $X(t)$, repeat steps 4 to 6, cycle $3\times M$ times, and obtain $3\times M$ CSP components with length N.

The flowchart of CSP is shown in Fig. 5.

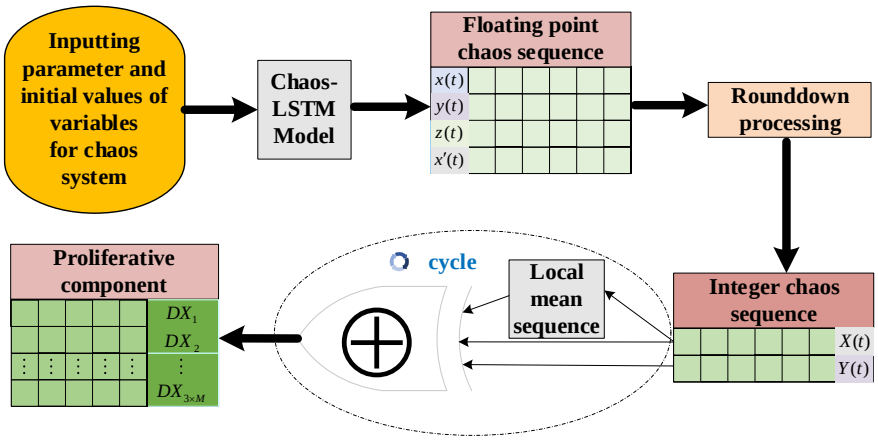

Fig. 5 Flowchart of CSP.

unedited

3.2 Randomness analysis of chaos proliferation sequences

Taking the chaos sequence generated and processed by the Lorenz system under the condition of parameter $c=2$, and initial values $x(0)=1, y(0)=2, z(0)=3$. Let $M=4$ and $N=500$, generate 12 CSP components $DX_j, j=1,2,\cdots,12$ with length 500 using the CSP algorithm. The CSP components are shown in Fig. 6.

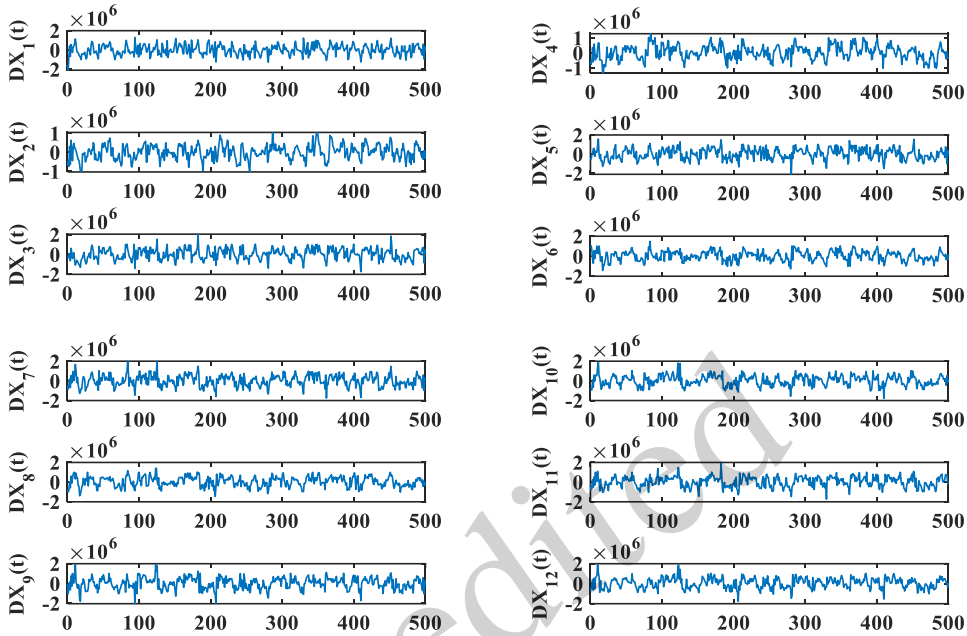

Fig. 6 Generated CSP components diagram.

Table 1 SE Complexity of sequences.

Sequence	SE Complexity
$DX_1(t)$	0.8904
$DX_2(t)$	0.8258
$DX_3(t)$	0.8565
$DX_4(t)$	0.8087
$DX_5(t)$	0.8580
$DX_6(t)$	0.8168
$DX_7(t)$	0.8531
$DX_8(t)$	0.8175
$DX_9(t)$	0.8549
$DX_{10}(t)$	0.8295
$DX_{11}(t)$	0.8429
$DX_{12}(t)$	0.8308
$X(t)$	0.8078

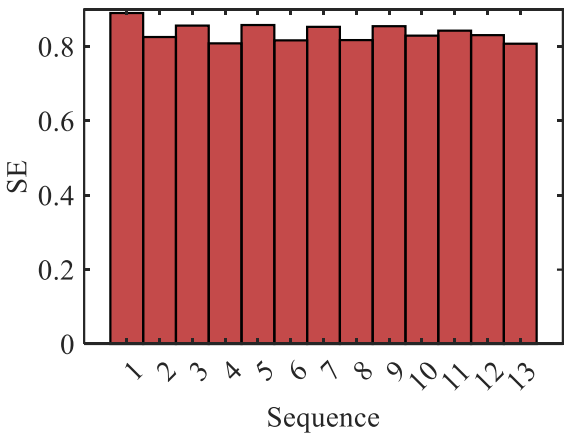

Fig. 7 The comparison of SE complexity of sequences.

Calculate the SE complexity of chaos sequence $X(t)$ and all chaos proliferation sequences, and conduct a comparative analysis, which is visually displayed in Table 1 and Fig. 7. In the coordinate axis shown in Fig.7, the vertical axis represents SE complexity, and the horizontal axis represents each sequence, that is, Sequence1–Sequence12 represent

unedited

DX_1 □ DX_{12}, and Sequence13 represents $X(t)$. From Table 1 and Fig. 7, the SE complexity of each chaos proliferation sequence is greater than the SE complexity of chaos sequence $X(t)$. This means that the CSP algorithm can not only infinitely multiply the original chaos sequence, but also that the extended chaos proliferation sequence is closer to a random sequence compared to the original chaos sequence.

To verify the randomness of chaos proliferation sequences, the chaos proliferation sequences with length 10^6 are selected for NIST tests and TestU01 tests (De la Fraga et al., 2021). In the NIST tests, the P-values of all 15 tests are greater than 0.01, and the TestU01 tests were also passed, indicating that the chaotic proliferation sequences have good randomness and belong to the random sequence (see supplementary materials, Section 1).

4 Secure Communication System and Experimental Analysis

For confidential objects with different data sizes, the Chaos-LSTM model and CSP algorithm in this paper provide adaptive encrypted sequences. The complexity of the encrypted sequences, compared to the original chaos sequences, is also significantly improved. Therefore, combining the Chaos-LSTM model and CSP algorithm with scrambling and diffusion algorithms to construct encryption algorithms can be used for encrypting various geographic information data.

Geographic information data refers to the general term for numbers, text, images, and graphics of geographical circles or environments, which contain the quantity, quality, distribution characteristics, connections, and patterns of inherent elements or substances. Digital images, a representative data structure, contain more information than text and sound, which are also the foundation of video formation. So, taking the encryption of color geographic information images with a grayscale of $L = 256$ and a size of $M \times N \times 3$ as an example, the structure of the geographic information encryption system based on Chaos-LSTM and CSP designed in this paper is shown in Fig. 8.

Unedited

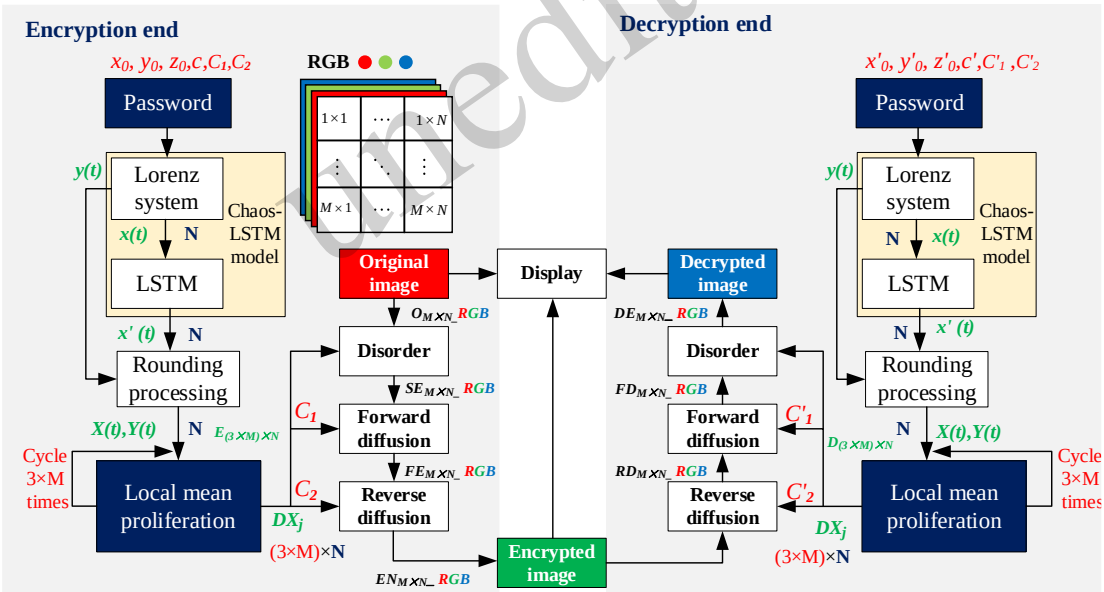

Fig. 8 The flowchart of the geographic information encryption system based on Chaos-LSTM and CSP.

In Fig. 8, $x_0, y_0, z_0, c, C_1, C_2$ is the encryption key and $x'_0, y'_0, z'_0, c', C'_1, C'_2$ is the decryption key, where the value range of the key is $c, c' \in [-1, 7.75], C_1, C'_1 \in [0, 255], C_2, C'_2 \in [0, 255]$. The specific process of the encryption system is as follows.

Step 1: Input the encryption key x_0, y_0, z_0, c into the Lorenz system to generate 3-dimensional floating-point chaos sequences $x(t), y(t), z(t)$ with N length.

Step 2: Input the sequence $x(t)$ into the Chaos-LSTM model and output a new chaos sequence $x'(t)$ with the same length as sequence $x(t)$.

Step 3: Convert floating-point chaos sequences

$x'(t), y(t)$ into integer chaos sequences $X(t), Y(t)$ through the rounding processing module.

Step 4: Input sequences $X(t), Y(t)$ into the local mean proliferation module to obtain the CSP component DX_j.

Step 5: Take the proliferation component DX_j as the chaos sequence $X(t)$, repeat Step 4, and cycle $3\times M$ times to obtain CSP components $DX_j, j=1,2,\cdots,3\times M$ with length N.

Step 6: Use CSP components DX_j as the encryption sequence $E_{(3\times M)\times N}$, and set the encryption key C_1, C_2. Scramble the row of the original image $O_{M\times N}_RGB$ to obtain image $SE_{M\times N}_RGB$, then perform forward diffusion to obtain image $FE_{M\times N}_RGB$, and reverse diffusion to obtain image $EN_{M\times N}_RGB$.

Step 7: Transfer the encrypted image to the decryption end for decryption, which process is the reverse of the encryption process, and display the images.

In Step 6, row scrambling, as shown in Eq. (9) is performed to obtain image $SE_{M\times N}_RGB$.

Among them, $O_{M\times N}_RGB$ is the original image matrix, $SE_{M\times N}_RGB$ is the scrambled image matrix, $\Updownarrow$ represents the matrix element exchange operation. $p=1,2,\cdots,M$, and $q=1,2,\cdots,floor(N/2)$ are rows and columns of matrix positions.

Perform forward diffusion as shown in Eq. (10) on scrambled images to obtain $FE_{M\times N}_RGB$.

$$
\begin{aligned}
SE_{M\times N}_R &= \begin{cases} O_{M\times N}_RGB\left(p, E_{(3\times M)\times N}(p,q)\right) \\ \Updownarrow \\ O_{M\times N}_RGB\left(p, E_{(3\times M)\times N}(p, N-q+1)\right) \end{cases}, \\
SE_{M\times N}_G &= \begin{cases} O_{M\times N}_RGB\left(p+M, E_{(3\times M)\times N}(p+M,q)\right) \\ \Updownarrow \\ O_{M\times N}_RGB\left(p+M,\ E_{(3\times M)\times N}(p+M, N-q+1)\right) \end{cases}, \\
SE_{M\times N}_B &= \begin{cases} O_{M\times N}_RGB\left(p+2\times M, E_{(3\times M)\times N}(p+2\times M,q)\right) \\ \Updownarrow \\ O_{M\times N}_RGB\left(p+2\times M,\ E_{(3\times M)\times N}(p+2\times M, N-q+1)\right) \end{cases}, \\
SE_{M\times N}_RGB &= [SE_{M\times N}_R; SE_{M\times N}_G; SE_{M\times N}_B].
\end{aligned}
\tag{9}
$$

$$
FE_{M\times N}_RGB = \begin{cases} C_1 \oplus E_{(3\times M)\times N}(u,v) \oplus SE_{M\times N}_RGB(u,v), v=1 \\ FE_{M\times N}_RGB(u,v-1) \oplus E_{(3\times M)\times N}(u,v) \oplus SE_{M\times N}_RGB(u,v), \\ v=2,\cdots,N \end{cases}
\tag{10}
$$

Among them, $FE_{M\times N}_RGB$ represents the positive diffusion image matrix, $\oplus$ represents the bitwise XOR operation, $u=1,2,\cdots,3\times M$ and v are rows and columns of matrix positions.

Reverse diffusion is performed on a positive diffusion image to obtain image $EN_{M\times N}_RGB$, which is shown in Eq. (11):

$$
EN_{M\times N}_RGB = \begin{cases} C_2 \oplus E_{(3\times M)\times N}(m,n) \oplus FE_{M\times N}\times RGB(m,n), n=N \\ EN_{M\times N}\times RGB(m,n+1) \oplus E_{(3\times M)\times N}(m,n) \oplus FE_{M\times N}\times RGB(m,n), \\ n=N-1,\cdots,2,1 \end{cases}
\tag{11}
$$

Among them, $EN_{M\times N}_RGB$ represents the reverse diffusion image matrix, which is the encrypted image matrix, $m=1,2,\cdots,3\times M$, and n represents the rows and columns of matrix positions.

The proposed encryption system in this paper

unedited

includes 32-bit chaotic system initial values and parameters x_0, y_0, z_0, c and 8-bit diffusion algorithm initial value C_1, C_2. The calculated key space size is $2^{32\times4}\times2^{8\times2}$, which is much larger than 2^{100}, indicating that it has the ability to resist exhaustive attacks.

To measure the performance of the secure communication system, known plaintext attack, image histogram, correlation, key sensitivity, and information entropy, an encryption performance comparison and encryption quality analysis were conducted.

4.1 Analysis of known plaintext attacks

All black and white images are often used to evaluate the protection ability of encryption systems against known plaintext attacks. Let $[x_0, y_0, z_0, c, C_1, C_2] = [x_0', y_0', z_0', c', C_1', C_2'] = [1,2,3,2,0,0]$; the key used in this paper defaults to this key. All black and white images are encrypted and decrypted by the encryption system as shown in Fig. 9. The results demonstrate that proposed encryption system can effectively protect against known plaintext attacks.

4.2 Image Histogram Analysis

Histogram analysis which reflects the distribution characteristics of pixel grayscale values in digital images, is performed on the geographic information images and the corresponding encrypted images, and is displayed in Fig. 10. From Fig. 10, the distribution of pixel grayscale values in the histograms of the geographic information images are uneven, indicating significant differences in the number of grayscale values in the geographic information images. After images are encrypted, the distribution of pixel grayscale values in the histogram is unified, and the pixel grayscale information is well hidden. It is difficult to find patterns in the use of grayscale values in the encrypted image and crack the encryption system.

4.3 Correlation analysis

The encryption system needs to break the high correlation between general geographic information images to ensure confidentiality and security. Taking geographic information remote sensing image A as an example, Fig.11 shows the correlation coefficients in various directions of the original and encrypted image.

Calculate the correlation between the adjacent pixels in Fig. 11, and which are shown in Table 2.

The correlation coefficients in Table 2 are all the average results of 1000 experiments, which shows that the correlation coefficients in image A are relatively high in all directions, with strong correlation, while those in the encrypted image are close to 0 in all directions, indicating an approximate lack of correlation.

unedited

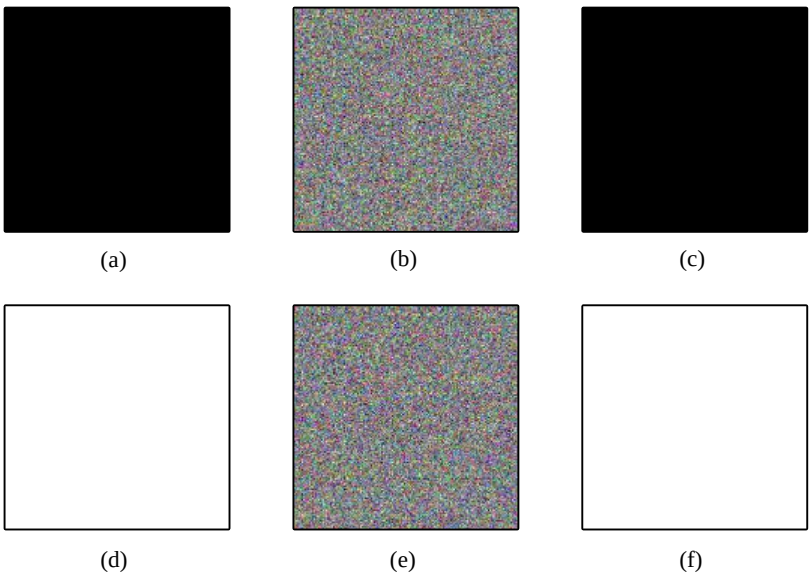

Fig. 9 Encryption experiments of all black image (256×256): (a)original; (b) encrypted; (c) decrypted; Encryption experiments of all white image (256×256): (d) original; (e) encrypted; (f) decrypted.

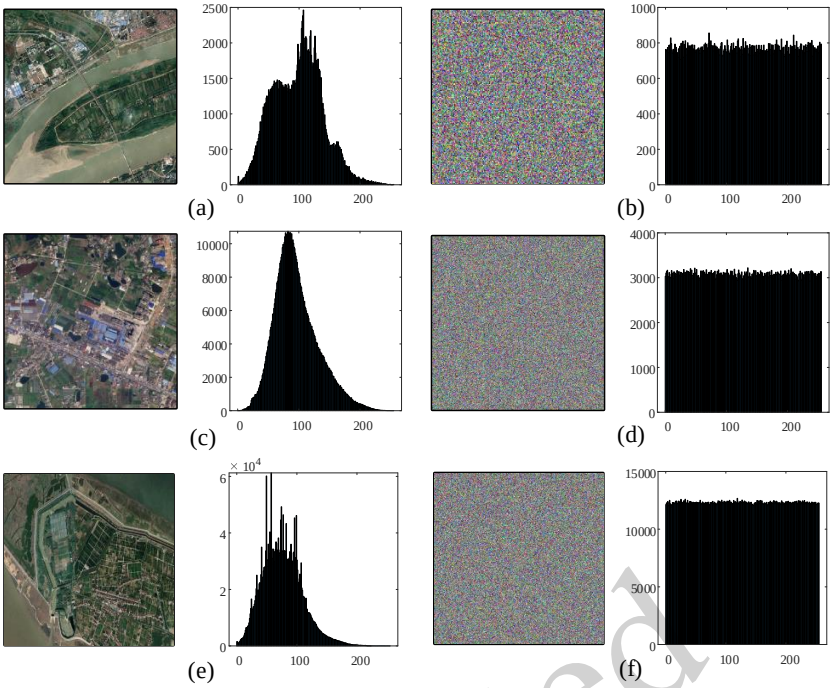

Fig. 10 Geographical information remote sensing image A and its histogram (a) original; (b) encrypted; image B and its histogram (c) original; (d) encrypted; image C and its histogram (e) original; (f) encrypted.

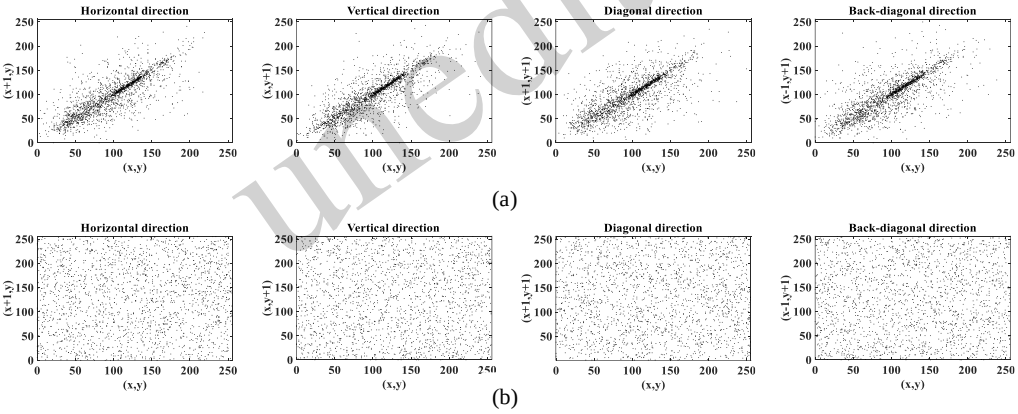

Fig. 11 Correlation coefficients in various directions of geographic information remote sensing image A: (a) original; (b) encrypted.

Table 2 Correlation coefficients

Image A	Horizontal	Vertical	Positive diagonal	Negative diagonal
Original	0.7710	0.7976	0.6864	0.7619
Encrypted	0.0149	-0.0179	0.0353	0.0328

4.4 Key sensitivity analysis

The key sensitivity analysis of encryption systems aims to prove that when the key changes, the encrypted image cannot be decrypted using the original key. Set the original key $K=[x_0,y_0,z_0,c,C_1,C_2]=[1,2,3,2,0,0]$ and make minor changes to the original key to obtain $K'=[x_0,y_0,z_0,c,C_1,C_2]=[1,2+10^{-12},3,2,0,0]$. As the results displayed in Fig. 12 show, the geographic information remote sensing image A is encrypted using the original key K , and then decrypted using K' .

unedited

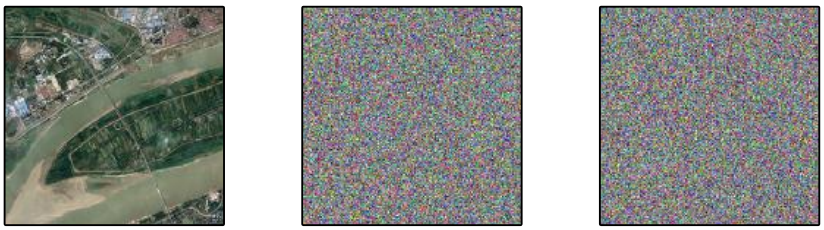

(a) (b) (c)

Fig. 12 Forward encryption and decryption of geographic information remote sensing image A: (a) original; (b) encrypted; (c) error decrypted.

On the contrary, Fig. 13 shows results showing that image A is encrypted using the key $K^{'}$, and then decrypted using the original key K.

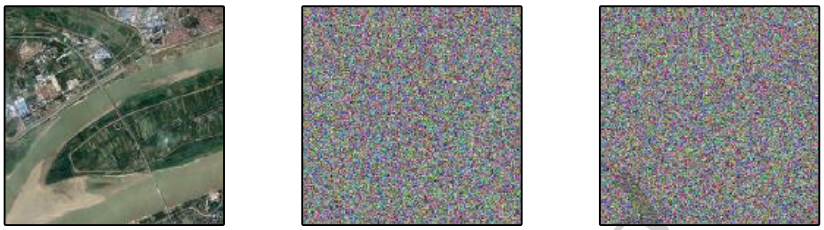

(a) (b) (c)

Fig. 13 Reverse encryption and decryption of geographic information remote sensing image A: (a) original; (b) encrypted image; (c) error decrypted

Figs. 12 and 13 show that there is only a small difference (10^{-12}) between the encryption key and the decryption key, but the decryption fails, reflecting the good key sensitivity of the constructed geographic information encryption system based on Chaos-LSTM and CSP.

4.5 Information entropy analysis

Information entropy H, as shown in Eq.(12), can reflect the uncertainty of image information.

$$H = -\sum_{i=0}^{L} p(i)\log_2 p(i), \tag{12}$$

where $L = 256$ and $p(i)$ represents the occurrence probability of grayscale value i, $i = 1, 2, \cdots, L$. The closer the H is to 8 (theoretical maximum value), the greater the uncertainty of the image information.

Table 3 Image information entropy

Image		H
Geographic information remote sensing image A（256×256）	Original	7.3368
	Encrypted	7.9992
Geographic information remote sensing image B（512×512）	Original	7.1322
	Encrypted	7.9997
Geographic information remote sensing image C（1024×1024）	Original	7.0290
	Encrypted	7.9999
All back image（256×256）	Original	0
	Encrypted	7.9992
All white image（256×256）	Original	0
	Encrypted	7.9991

From Table 3, the H of the original images is significantly less than 8, while that of the encrypted images is close to 8, indicating that the encrypted images have high uncertainty and good confidentiality effects.

4.6 Comparison of encryption performance

The number of pixels change rate (NPCR) refers to the proportion of different pixels in two images to the total number of pixels. The unified average changing intensity (UACI) refers to the average value of the ratio of the difference between all corresponding pixel positions in two images and the maximum difference (Rehman et al., 2018).

unedited

We have encrypted the image Lena using the proposed algorithm and the algorithms proposed in references RF1 (Hosseinzadeh et al., 2019), RF2 (Wu et al., 2015), and RF3 (Wu et al., 2016). It is easy to conclude that our proposed method has a good confidentiality performance (see supplementary materials, Section 2).

4.7 Encryption quality analysis

The encryption quality analysis is conducted on the encryption algorithm proposed in this paper, including the mean squared error (MSE), the peak signal-to-noise ratio (PSNR), the structural similarity index (SSIM), the chi-square test, and the floating frequency (Murillo-Escobar et al., 2019) (see supplementary materials, Section 3).

5 Hardware circuit experiment

The experimental environment is based on the XILINX ZYNQ7000 platform, which includes the dual-core ARM Cortex-A9 component and the FPGA programmable logic component. The geographic information encryption system formed by combining chaotic encryption sequences with scrambling and diffusion algorithms is mapped to ZYNQ. The experimental results are shown in Fig. 14, and the hardware resources used in the experiment are shown in Table 4.

The display screen in Fig. 14 displays the generated images from the ZYNQ experimental platform, and the images are exported as shown in Fig. 15, where, (a) is geographic information remote sensing image A, (b) is the encrypted image, and (c) is the decrypted image. The encrypted image is completely inconsistent with the original image as shown by comparing (a) and (b); the original features of the image are hidden. The decrypted image is consistent with the original image when comparing (a) and (c), and the image is fully restored through the decryption circuit.

Table 4 Utilization of the FPGA hardware resources using Zynq7000(xc7z020-2clg400I)

Resource	Used	Utilization
LUT	5684	10.68%
LUTRAM	533	3.06%
FF	8843	8.31%
BRAM	66	47.14%
IO	9	7.20%
BUFG	2	6.25%
MMCM	1	25%

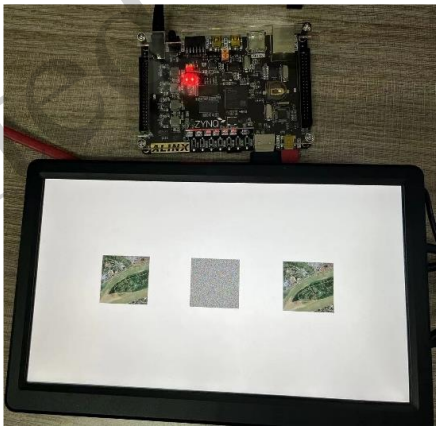

Fig. 14 Implementation and display of encryption system on ZYNQ experimental platform and screen.

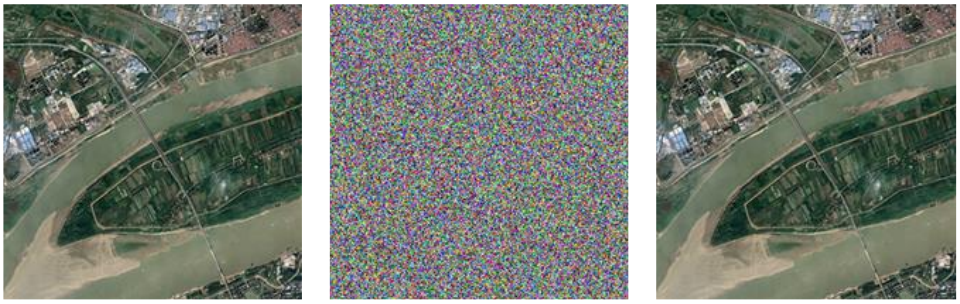

(a) (b) (c)

Fig. 15 Images in the display screen (a) original; (b) encrypted; (c) decrypted.

The proposed encryption system can perform secure communication correctly, and experimental and image data information can be hidden without losing data information. An excellent practical application effect is further proved by the hardware circuit experiment, which means the geographic information encryption system based on Chaos-LSTM and CSP can be applied to multiple encryption scenarios.

6 Conclusion

To ensure the security and adaptability of chaotic encryption communication, a geographic information

unedited

encryption system based on Chaos-LSTM and CSP is proposed in this paper, which is implemented on the ZYNQ platform. The encryption system's excellent confidentiality performance and practical application effects are proved by software testing and hardware experiments. The advantages and contributions of the proposed encryption system are as follows:

1. In chaotic encryption algorithms, the complexity of chaotic sequences determines the encryption performance. This paper combines chaotic systems and LSTM neural networks to construct the Chaos-LSTM model, avoiding the potential risk of output sequence periodization due to changes in the initial state and parameters of the chaotic system. The chaotic sequences output by the proposed Chaos-LSTM model have higher SE complexity compared to the chaotic sequences output by the original chaotic system. There is no need for chaotic systems to output long chaotic sequences, avoiding the periodicity that may occur due to excessively long chaotic sequences, and the new chaotic sequences have higher SE complexity.

2. The limited computational accuracy effect of computers can lead to periodicity in the output sequence of chaotic systems. The longer the chaotic sequence output of the chaotic system, the greater the possibility of periodicity. This paper proposes and constructs the CSP algorithm for chaotic sequences. Through this algorithm, only a portion of the output sequences of the chaotic system need to be selected to proliferate sufficient chaotic sequences for encryption.

3. The encryption system constructed in this paper can generate adaptive chaotic encryption sequences for encrypted objects, which can be applied to various encryption scenarios.

Future research direction: The constructed encryption system is currently mainly used for geographic information data encryption, and we will expand its application scenarios in future research. When the amount of information in the encrypted object is large, the encryption and decryption speed of the system is still relatively slow. We will continue to improve the algorithm and optimize the hardware to enhance the efficiency of the system's encrypted communication.

Contributors

Jia DUAN designed the research. Lunyun HU collected the data. Qiumei XIAO and Meiting LIU processed the data. Qiumei XIAO drafted the manuscript, Wenxin Yu helped organize the manuscript.

Conflict of interest

Jia DUAN, Luanyun HU, Qiumei XIAO, Meiting LIU and Wenxin Yu declare that they have no conflict of interest.

References

Alexan W, Elkandoz M, Mashaly M, et al., 2023. Color image encryption through chaos and KAA map. *IEEE Access*, 11:11541-11554. https://doi.org/10.1109/ACCESS.2023.3242311

Cao Y, Zhao YL, Wang Q, et al., 2022. The evolution of quantum key distribution networks: On the road to the qinternet. *IEEE Commun Surv Tutorials*, 24(2):839-894. https://doi.org/10.1109/COMST.2022.3144219

Chen X, Qian S, Yu F, et al., 2020. Pseudorandom number generator based on three kinds of four-wing memristive hyperchaotic system and its application in image encryption. *Complexity*, 2020:8274685. https://doi.org/10.1155/2020/8274685

De la Fraga LG, Mancillas-López C, Tlelo-Cuautle E, 2021. Tlelo-Cuautle E. Designing an authenticated Hash function with a 2D chaotic map. *Nonlinear Dyn*, 104(4):4569-4580. https://doi.org/10.1007/s11071-021-06491-3

De la Fraga LG, Ovilla-Martínez B, Tlelo-Cuautle E, 2023. Echo state network implementation for chaotic time series prediction. *Microprocessors Microsyst*, 103:104950. https://doi.org/10.1016/j.micpro.2023.104950

Gabr M, Korayem Y, Chen YL, et al., 2023. R^3– rescale, rotate, and randomize: a novel image cryptosystem utilizing chaotic and hyper-chaotic systems. *IEEE Access*, 11:119284-119312. https://doi.org/10.1109/ACCESS.2023.3326848

Gonzalez-Zapata AM, De la Fraga LG, Ovilla-Martinez B, et al., 2023. Enhanced FPGA implementation of Echo State Networks for chaotic time series prediction. *Integration*, 92:48-57. https://doi.org/10.1016/j.vlsi.2023.05.002

Hosseinzadeh R, Zarebnia M, Parvaz R, 2019. Hybrid image encryption algorithm based on 3D chaotic system and choquet fuzzy integral. *Opt Laser Technol*, 120:105698. https://doi.org/10.1016/j.optlastec.2019.105698

Irfan M, Ali A, Khan MA, et al., 2020. Pseudorandom number generator (PRNG) design using hyper-chaotic modified robust logistic map (HC-MRLM). *Electronics*, 9(1):104. https://doi.org/10.3390/electronics9010104

Jia YQ, Shelhamer E, Donahue J, et al., 2014. Caffe: Convolutional architecture for fast feature embedding. Proc 22nd ACM Int Conf on Multimedia, p.675-678. https://doi.org/10.1145/2647868.2654889

Lin HR, Wang CH, Cui L, et al., 2022. Hyperchaotic memristive ring neural network and application in medical image

unedited

encryption. *Nonlinear Dyn*, 110(1):841-855. https://doi.org/10.1007/s11071-022-07630-0

Liu XC, Mou J, Zhang YS, et al., 2024. A new hyperchaotic map based on discrete memristor and meminductor: dynamics analysis, encryption application, and dsp implementation. *IEEE Trans Ind Electron*, 71(5):5094-5104. https://doi.org/10.1109/TIE.2023.3281687

Lorenz EN, 1963. Deterministic nonperiodic flow. *J Atmos Sci*, 20(2):130-141. https://doi.org/10.1175/1520-0469(1963)020<0130:DNF>2.0.CO;2

Man ZL, Li JQ, Di XQ, et al., 2021. Double image encryption algorithm based on neural network and chaos. *Chaos, Solitons Fractals*, 152:111318. https://doi.org/10.1016/j.chaos.2021.111318

Martins P, Sousa L, Mariano A, 2017. A survey on fully homomorphic encryption: An engineering perspective. *ACM Comput Surv*, 50(6):83. https://doi.org/10.1145/3124441

Murillo-Escobar MA, Meranza-Castillón MO, López-Gutiérrez RM, et al., 2019. Suggested integral analysis for chaos-based image cryptosystems. *Entropy*, 21(8):815. https://doi.org/10.3390/e21080815

Murillo-Escobar MA, Cruz-Hernández C, Cardoza-Avendaño L, et al., 2022. Multibiosignal chaotic encryption scheme based on spread spectrum and global diffusion process for e-health. *Biomed Signal Process Control*, 78:104001. https://doi.org/10.1016/j.bspc.2022.104001

Pareschi F, Rovatti R, Setti G, 2012. On statistical tests for randomness included in the NIST SP800-22 test suite and based on the binomial distribution. *IEEE Trans Inf Forensics Secur*, 7(2):491-505. https://doi.org/10.1109/TIFS.2012.2185227

Rehman AU, Liao XF, Ashraf R, et al., 2018. A color image encryption technique using exclusive-OR with DNA complementary rules based on chaos theory and SHA-2. *Optik*, 159:348-367. https://doi.org/10.1016/j.ijleo.2018.01.064

Sahu HK, Jadhav V, Sonavane S, et al., 2016. Cryptanalytic attacks on international data encryption algorithm block cipher. *Defence Sci J*, 66(6). https://doi.org/10.14429/dsj.66.10798

Teh JS, Alawida M, Sii YC, 2020. Implementation and practical problems of chaos-based cryptography revisited. *J Inf Security Appl*, 50:102421. https://doi.org/10.1016/j.jisa.2019.102421

Tezcan C, 2022. Key lengths revisited: GPU-based brute force cryptanalysis of DES, 3DES, and PRESENT. *J Syst Archit*, 124:102402. https://doi.org/10.1016/j.sysarc.2022.102402

Tlelo-Cuautle E, Díaz-Muñoz JD, González-Zapata AM, et al., 2020. Chaotic image encryption using hopfield and hindmarsh–rose neurons implemented on FPGA. *Sensors*, 20(5):1326. https://doi.org/10.3390/s20051326

Ullah S, Zheng JB, Din N, et al., 2023. Elliptic Curve Cryptography; Applications, challenges, recent advances, and future trends: A comprehensive survey. *Comput Sci Rev*, 47:100530. https://doi.org/10.1016/j.cosrev.2022.100530

Wan YJ, Gu SQ, Du BX, 2020. A new image encryption algorithm based on composite chaos and hyperchaos combined with DNA coding. *Entropy*, 22(2):171. https://doi.org/10.3390/e22020171

Wu XJ, Kan HB, Kurths J, 2015. A new color image encryption scheme based on DNA sequences and multiple improved 1D chaotic maps. *Appl Soft Comput*, 37:24-39. https://doi.org/10.1016/j.asoc.2015.08.008

Wu XJ, Wang DW, Kurths J, et al., 2016. A novel lossless color image encryption scheme using 2D DWT and 6D hyperchaotic system. *Inf Sci*, 349-350:137-153. https://doi.org/10.1016/j.ins.2016.02.041

Xiong PY, Jahanshahi H, Alcaraz R, et al., 2021. Spectral entropy analysis and synchronization of a multi-stable fractional-order chaotic system using a novel neural network-based chattering-free sliding mode technique. *Chaos, Solitons Fractals*, 144:110576. https://doi.org/10.1016/j.chaos.2020.110576

Xu SC, Wang XY, Ye XL, 2022. A new fractional-order chaos system of Hopfield neural network and its application in image encryption. *Chaos, Solitons Fractals*, 157:111889. https://doi.org/10.1016/j.chaos.2022.111889

Yan S, Gu Z, Park JH, et al., 2023. Synchronization of delayed fuzzy neural networks with probabilistic communication delay and its application to image encryption. *IEEE Trans Fuzzy Syst*, 31(3):930-940. https://doi.org/10.1109/TFUZZ.2022.3193757

Yu F, Zhang ZN, Shen H, et al., 2022. FPGA implementation and image encryption application of a new PRNG based on a memristive Hopfield neural network with a special activation gradient. *Chin Phys B*, 31(2):020505. https://doi.org/10.1088/1674-1056/ac3cb2

Yu Y, Si XS, Hu CH, et al., 2019. A review of recurrent neural networks: LSTM cells and network architectures. *Neural Comput*, 31(7):1235-1270. https://doi.org/10.1162/neco_a_01199

List of supplementary materials

1 NIST tests and TestU01 tests

2 Comparison of encryption performance

3 Encryption Quality analysis

Table S1 NIST and TestU01 tests of chaos proliferation sequences

Table S2 Compare in NPCR, UACI and Information entropy

Table S3 Quality metrics' analysis

Fig. S1 Lena: (a) Plain image P; (b) Encrypted image E

Fig. S2 CFF and its mean: (a) R-component of P, (b) G-component of P, (c) B-component P, (d) R-component of E, (e) G-component of E, and (f) B-component of E

Fig. S3 RFF and its mean: (a) R-component of P, (b) G-component of P, (c) B-component P, (d) R-component of E, (e) G-component of E, and (f) B-component of E

unedited